Author Manuscript

# North–South Plasma Asymmetry across Mercury's Near-tail Current Sheet

**Jun Zhong[1], Lianghai Xie[2,8], Lou-Chuang Lee[3,4], James A. Slavin[5], Jim M. Raines[5], Ryan M. Dewey[5], Wing-Huen Ip[6], Yoshifumi Saito[7], Yong Wei[1]**

[1]Key Laboratory of Earth and Planetary Physics, Institute of Geology and Geophysics, Chinese Academy of Sciences, Beijing, China

[2] National Space Science Center, Chinese Academy of Sciences, Beijing, China

[3]Institute of Earth Sciences, Academia Sinica, Taipei, Taiwan

[4]State Key Laboratory of Lunar and Planetary Sciences, Macau University of Science and Technology, Macau, China

[5]Department of Climate and Space Sciences and Engineering, University of Michigan, Ann Arbor, Michigan, USA

[6]Graduate Institute of Astronomy, National Central University, Taoyuan, Taiwan

[7]Institute of Space and Astronautical Science, Japan Aerospace Exploration Agency, Kanagawa, Japan

[8]Joint Research and Development Center of Chinese Science Academy and Shen County, Shandong, China

Corresponding to: Jun Zhong (j.zhong@mail.iggcas.ac.cn); Lianghai Xie (xielianghai@nssc.ac.cn)

**Key Points:**

- North–south asymmetries exist in Mercury's magnetotail.
- Both the IMF $B_X$ polarity and intrinsic offset dipole magnetic field control the north–south density asymmetry in Mercury's tail.
- The IMF Parker spiral results in a dawnside preference for the plasma asymmetric current sheet.

This is the author manuscript accepted for publication and has undergone full peer review but has not been through the copyediting, typesetting, pagination and proofreading process, which may lead to differences between this version and the Version of Record. Please cite this article as doi: 10.1029/2023GL106266.

This article is protected by copyright. All rights reserved.

Author Manuscript

**Abstract**

Among nearly 300 near-Mercury tail current sheet crossings performed by the MESSENGER spacecraft, we identified 37 traversals of an asymmetric current sheet, wherein the lobe densities on opposite sides differ by a factor of three or more. These asymmetric current sheet crossings primarily occur on the dawnside. A global magnetohydrodynamic (MHD) simulation was found to be in excellent agreement with the observations. The results suggest that the north–south density asymmetry is caused by solar wind entering via an upstream-connected window in one hemisphere. Furthermore, the Parker spiral interplanetary magnetic field (IMF) controls the near-tail density asymmetries, whereas Mercury's offset dipole magnetic field controls those in mid- or distant-tail regions. We propose that hemispheric asymmetries in Mercury's magnetospheric convection occur under strong IMF conditions.

**Plain Language Summary**

Mercury possesses a small magnetosphere owing to its weak planetary magnetic field and strong interactions with the solar wind in the inner heliosphere. The transport process of the solar wind mass and energy into its magnetosphere remains unclear. Previous MESSENGER observations suggest that although the Earth-like plasma mantle is detected inside the near-tail magnetopause in normal IMF magnitudes, it is not a permanent feature of Mercury's magnetosphere. Here we report, for the first time, that solar wind ions can enter deep into the near-tail region via an upstream-connected window in one hemisphere and form a density-asymmetric current sheet under strong IMF conditions. Through MHD simulations, we revealed tail dawn–dusk asymmetries during the transport of solar wind plasma. Advanced data expected from BepiColombo will further improve our understanding of the solar wind–magnetosphere coupling.

This article is protected by copyright. All rights reserved.

Author Manuscript

## 1 Introduction

Mercury has a small magnetosphere, approximately 5% the size of the Earth's (*Winslow et al.*, 2013; *Zhong et al.*, 2015), formed by the interaction of solar wind in the inner heliosphere with a weak global dipolar magnetic field, which is ~195 nT-$R_M^3$ (*Anderson et al.*, 2011). The basic structure of Mercury's magnetosphere is analogous to that of Earth's; it has a hemispherical dayside magnetosphere, high-latitude cusps, and a stretched magnetotail on the nightside. Given the low Alfvénic Mach number of the solar wind in the inner heliosphere (*Slavin and Holzer*, 1979), the reconnection-driven minutes-timescale "Dungey cycle" is regarded as the primary mode of plasma entering and circulating in Mercury's magnetosphere (*Slavin et al.*, 2021).

MESSENGER observations have shown that magnetic reconnection can be readily triggered at Mercury's dayside magnetopause, even under an extremely small magnetic shear (*DiBraccio et al.*, 2013). It is commonly observed as flux transfer events (FTEs) or "FTE showers" (*Slavin et al.*, 2010; *Slavin et al.*, 2012; *Leyser et al.*, 2017; *Sun et al.*, 2020; *Zhong et al.*, 2020). The newly created open field lines that connect the IMF to the planetary magnetic field provide a direct channel through which solar wind can enter the magnetic cusps (*Raines et al.*, 2014; *Poh et al.*, 2016; *Raines et al.*, 2022). As open field lines carry the solar wind plasma into the magnetotail, a boundary layer loaded with anti-sunward magnetosheath-like plasma, called plasma mantle, forms inside the high-latitude magnetotail (*DiBraccio et al.*, 2015). Finally, these high-latitude mantle plasmas undergo convection and enter the distant-tail plasma sheet through tail reconnection. Statistical analysis has shown that the plasma mantle in the near-Mercury high-latitude tail is typically detected under normal IMF magnitudes; however, it is not a permanent feature of its magnetosphere (*Jasinski et al.*, 2017).

The main feature of Mercury's near-tail lobes is a plasma hole region with a tenuous or nearly absent ion flux (*Raines et al.*, 2011). Relatively thick lobes are

This article is protected by copyright. All rights reserved.

Author Manuscript

occasionally separated by a thin current sheet (150–300 km thick), which is comparable to the gyroradii of protons (*Poh et al.*, 2017). Here, we report the observations of north–south asymmetry in lobe densities on opposite sides of the near-planet tail current sheet. Combined with a global MHD simulation, we suggest that the north–south density asymmetry is caused by the deep penetration of solar wind on the dawnside via an upstream-connected window in one hemisphere, which depends on the polarity of the IMF sector. The results suggest that in addition to the usual plasma mantle transport, the direct ingress of upstream solar wind plasma into the magnetotail is also crucial for solar wind-magnetosphere coupling, especially under strong IMF conditions.

## 2 Observations

We used magnetic field data (20 vectors $s^{-1}$) from the Magnetometer (MAG; (*Anderson et al.*, 2007) and ion plasma data (complete energy per charge up to 13 keV/e in 10 s) from the Fast Imaging Plasma Spectrometer (FIPS; (*Andrews et al.*, 2007) onboard the MESSENGER spacecraft. FIPS measured the energy per charge (E/q) of ions from 46 eV/e to 13.3 keV/e, sweeping through these energies to create a full energy spectrum approximately every 10 s. It had a large instantaneous field of view (FOV) of 1.4 π sr, although ~0.25 π sr was blocked by the spacecraft and its sunshade. We calculate proton densities and temperatures by following the procedure established in papers *Raines et al.* (2011), *Gershman et al.* (2013), and *Dewey et al.* (2018; 2020): we compute moments of the 1D velocity distribution function (VDF, i.e., phase space density as a function of E/q) via numerical integration. This approach assumes any flows present are subsonic since the 1D VDF has been integrated over the FIPS FOV. For a discussion of potential FOV effects and this subsonic assumption, we refer readers to these papers. These 1D VDFs are available on the NASA PDS.

The data are presented in the aberrated Mercury solar magnetospheric (MSM)

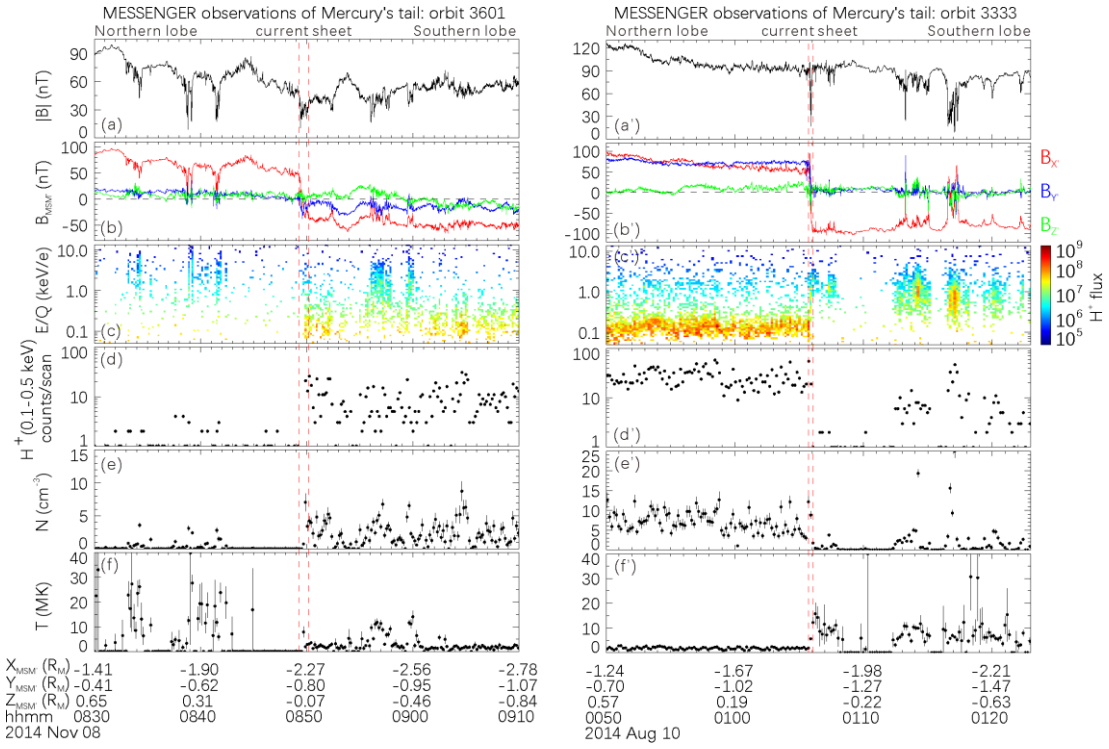
This article is protected by copyright. All rights reserved.

Author Manuscript

coordinate system, assuming a radial solar wind velocity of 400 km/s. The coordinate system is centered on Mercury's internal dipole, with the x-axis approximately in the opposite direction to the solar wind flow in Mercury's frame, the z-axis parallel to the planetary spin axis and positive in the northward direction, and the y-axis completing the right-handed set (*Anderson et al.*, 2011).

### 2.1 Examples of North–South Asymmetry Across Current Sheet

Figure 1 shows an overview of two tail current sheet traversals observed by MESSENGER during orbits 3601 and 3333. Both tail current sheet crossings occurred on the dawnside and from the northern ($B_{X'} > 0$) to the southern ($B_{X'} < 0$) lobe. The lobes are characterized by a strong magnetic field magnitude |B| and low fluctuations in the positive (negative) $B_{X'}$ component for the northern (southern) lobe. The complete current sheet crossings can be identified by a positive-to-negative reversal in $B_{X'}$ and a decrease in |B| during 08:49:18−08:49:53 and 01:05:48−01:06:02 UT, respectively. The rapid current sheet crossings suggest that the current sheets are relatively thin and/or moving rapidly past the spacecraft.




This article is protected by copyright. All rights reserved.

Author Manuscript

**Figure 1.** Two tail current sheet crossings exhibiting plasma asymmetries observed by MESSENGER. (a, a') Magnetic field magnitude. (b, b') Three components of the magnetic field in the aberrated MSM coordinates. (c, c') FIPS $H^+$ differential flux in $cm^{-2}$ $sr^{-1}$ $s^{-1}$ $keV^{-1}$. (d, d') Count rate of 0.1−0.5 keV $H^+$. (e, e') and (f, f') Calculated $H^+$ number density and temperature for each scan. The spacecraft's location is indicated at the bottom of the figure. Red vertical dashed lines mark the periods of current sheet crossings.

The key feature of these two events is the difference in the plasma properties between the northern and southern lobes. During orbit 3601, MESSENGER observed that the northern lobe had tenuous or lack of ion flux, which is a regular plasma feature of Mercury's tail lobe. However, in the southern lobe, a remarkably cold and dense ion population with flux energy ranging from tens of electron volts to 0.5 keV was observed (Figure 1c). The energy range of this ion population was lower than those of the magnetosheath and plasma sheet. The southern lobe showed 0.1–0.5 keV $H^+$ count rates of ~10 counts/scan, in contrast to only 1 count/scan for the northern lobe (Figure 1d). The calculated $H^+$ number densities (Figure 1e) in the southern lobe (> 3 $cm^{-3}$) were substantially higher than those in the northern lobe (< 1 $cm^{-3}$). The temperature of these dense ions in the lobe were relatively cold (< 5 MK), compared with the hot plasma sheet populations (> 10 MK) occasionally encountered (Figure 1f). During orbit 3333, north–south density asymmetries were also observed. However, cold dense ions were abundant in the northern lobe.

Additionally, in the lobe with higher density, a clear dawn–dusk oriented magnetic field was observed. During orbit 3601, the southern lobe field exhibits a remarkable dawnward component ($-B_Y$), although the field displays intermittent fluctuations (Figure 1b). In some periods, e.g., 08:23-08:24 UT, the $-B_Y$ component reached a peak strength of 30 nT, representing 50% of the magnitude of $B_X$ component. During orbit 3333, a strong and steady duskward $B_Y$ component persists

This article is protected by copyright. All rights reserved.

Author Manuscript

in the northern lobe, even larger than the $B_X$ component (Figure 1b').

### 2.2 Dawn–Dusk Distributions

Poh et al. (2017) identified ~320 MESSENGER central plasma sheet crossings in the near-planet tail during the spacecraft's orbital mission. It is impossible to simultaneously sample both the north and south tail lobes with a single spacecraft. To minimize the temporal and spatial variations of plasma in the lobe region, we selected the current sheet crossings based on criteria: (1) the central plasma sheet crossing was less than 10 minutes in duration so that both lobes could be observed near in time to each other; (2) the spatial variation of the spacecraft position in the X' and Z' directions before and after current sheet crossing are both less than 0.5 $R_M$. This resulted in a total of 202 traversals of current sheet. To obtain sufficient number of events for statistical analysis, these criteria are somewhat arbitrary; however, the results did not qualitatively change when smaller thresholds were considered.

We derived the lobe $H^+$ number density adjacent to each side of the current sheet crossing over 5 minutes (gray dots in Figure 2a). In the calculations, we used only FIPS scans with plasma beta lower than 0.5 in order to avoid any plasma sheet populations in the lobe. To identify cases of north-south asymmetry, we applied the following criteria: ion number density on opposite sides of the current sheet differ by at least a factor of 3, and number density on the denser-side greater than 0.6 $cm^{-3}$ (4 times the median). We identified 24 and 13 such cases with denser plasma in the southern (blue circles) and northern lobes (red circles), respectively. A total of 30 of the 37 asymmetric current sheet events were observed on the dawnside of the tail (Figure 2b). Note that the 202 search orbits are almost evenly distributed on the dusk and dawn sides, with 98 and 104 orbits respectively. The greater number of asymmetric current sheet events observed on the dawnside therefore corresponds to a higher occurrence rate there.

This article is protected by copyright. All rights reserved.

Author Manuscript

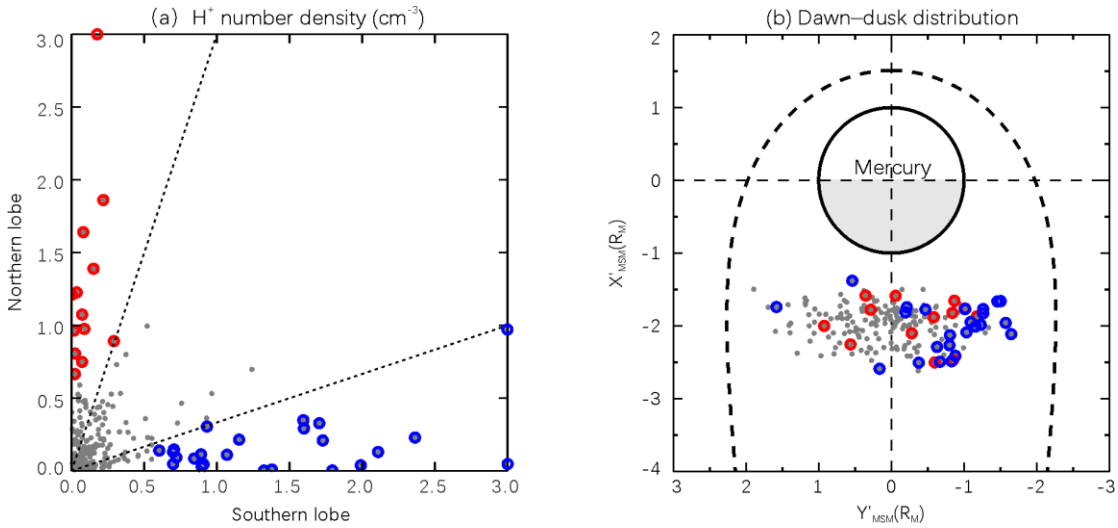



**Figure 2.** Statistical results of the northern and southern lobes for 202 traversals of the near-Mercury tail current sheet. (a) Calculated $H^+$ number density for 5 min averages of FIPS energy-per-charge scans in two lobes adjacent to each side of the current sheet. (b) Projection of the current sheet crossings onto the equatorial plane in aberrated MSM coordinates relative to Mercury's surface (circle) and the average magnetopause obtained from the 3D model (dashed curve) (*Zhong et al.*, 2015). Blue and red circles denote north-south asymmetry events with three times higher densities in the southern and northern lobes, respectively. Gray dots represent all analyzed 202 traversals of the current sheet center.

### 2.3 Correlations with IMF

Owing to the lack of an upstream IMF monitor, we used the average value of the magnetic field measured over 10 min just upstream of the inbound and outbound bow shocks to determine the upstream IMF conditions. The time period between upstream measurements and tail current sheet crossings was typically ~2 hr. Over a 2 hr interval, *James et al.* (2017) demonstrated that the IMF magnitude had an ~25% probability of varying by 20%–35%, and its hemispheric polarity (sunward and antisunward) had a much lower likelihood of changing. Nevertheless, the overall probability of north-south polarity changes after 2 hr exceeds 50%.

This article is protected by copyright. All rights reserved.

Author Manuscript

Figure 3a and 3b show the histograms of the IMF magnitude and $B_Z$, respectively. For 202 orbit events (green), the median IMF strength and $B_Z$ was ~27 nT and −3 nT, respectively. This median IMF strength is greater than the value of ~23 nT for all tail crossings where the current sheet may be detected (black) [Figure 8a in *Zhong et al.* (2023)]. These suggest that here selected 202 thin current sheet events tend to occur under strong and southward IMF. The north–south asymmetry events (purple) meanwhile occurred under even stronger IMF conditions, with median IMF strength ~31 nT, but smaller magnitude of southward component.

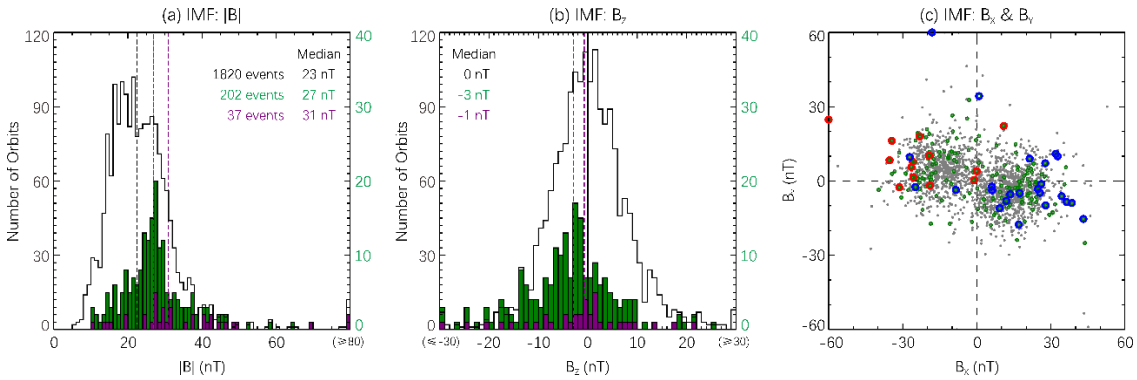



**Figure 3**. Statistical properties of IMF. (a) Histograms of the IMF magnitude. (b) Histograms of the IMF $B_Z$. (c) IMF $B_X$ and $B_Y$. Black: 1820 tail equator crossing events with $(X'_{MSM}{}^2+Y'_{MSM}{}^2)^{0.5} > 1.5$ $R_M$ and MLT = 21-03 h (*Zhong et al.*, 2023). Green: 202 thin current sheet crossing events. Purple: 37 north-south asymmetry events. Blue and red circles: north-south asymmetry events with higher densities in the southern and northern lobes, respectively.

The IMF generally has two types of sector structures: toward (IMF $B_X > 0$ and $B_Y < 0$) and away (IMF $B_X < 0$ and $B_Y > 0$) from the Sun. The sense of north–south asymmetry is correlated with the IMF sector structure (Figure 3c). Events with higher density in the southern (northern) lobe predominately occurred in the toward (away) sector.

This article is protected by copyright. All rights reserved.

Author Manuscript

## 3 Comparisons with Simulation

A global MHD simulation is helpful for understanding the entering of solar wind into the near-Mercury tail. We used the Space Weather Modeling Framework (SWMF) tool (*Tóth et al.*, 2012) to perform such a simulation, with parameters similar to those adopted by *Jia et al.* (2015). The center of the intrinsic dipole magnetic field is offset northward by 0.2 $R_M$ from the equator, with an equatorial surface field strength of 195 nT. The planet was considered to have a conductive iron core with a radius of 0.8 $R_M$. The region above the core was regarded as a highly resistive mantle. The computational domain was set to $-15\ R_M \le X \le 5\ R_M$, $-10\ R_M \le Y \le 10\ R_M$, and $-10\ R_M \le Z \le 10\ R_M$ in MSO coordinates. A non-uniform spherical grid was used, with a minimum grid size of 0.01 $R_M$ near the surface of the planet and a maximum grid size of 0.27 $R_M$ near the outer boundary. Based on the IMF properties shown in Figure 3, we choose two sets of IMF, $\mathbf{B}_{IMF}$ = [30, −10, −5] nT and $\mathbf{B}_{IMF}$ = [−30, 10, −5] nT, for the IMF toward and away sectors, respectively. The number density, speed, and temperature of the solar wind were set to their typical values of 50 $cm^{-3}$, 400 km/s, and $1 \times 10^5$ K, respectively.

This article is protected by copyright. All rights reserved.

Author Manuscript

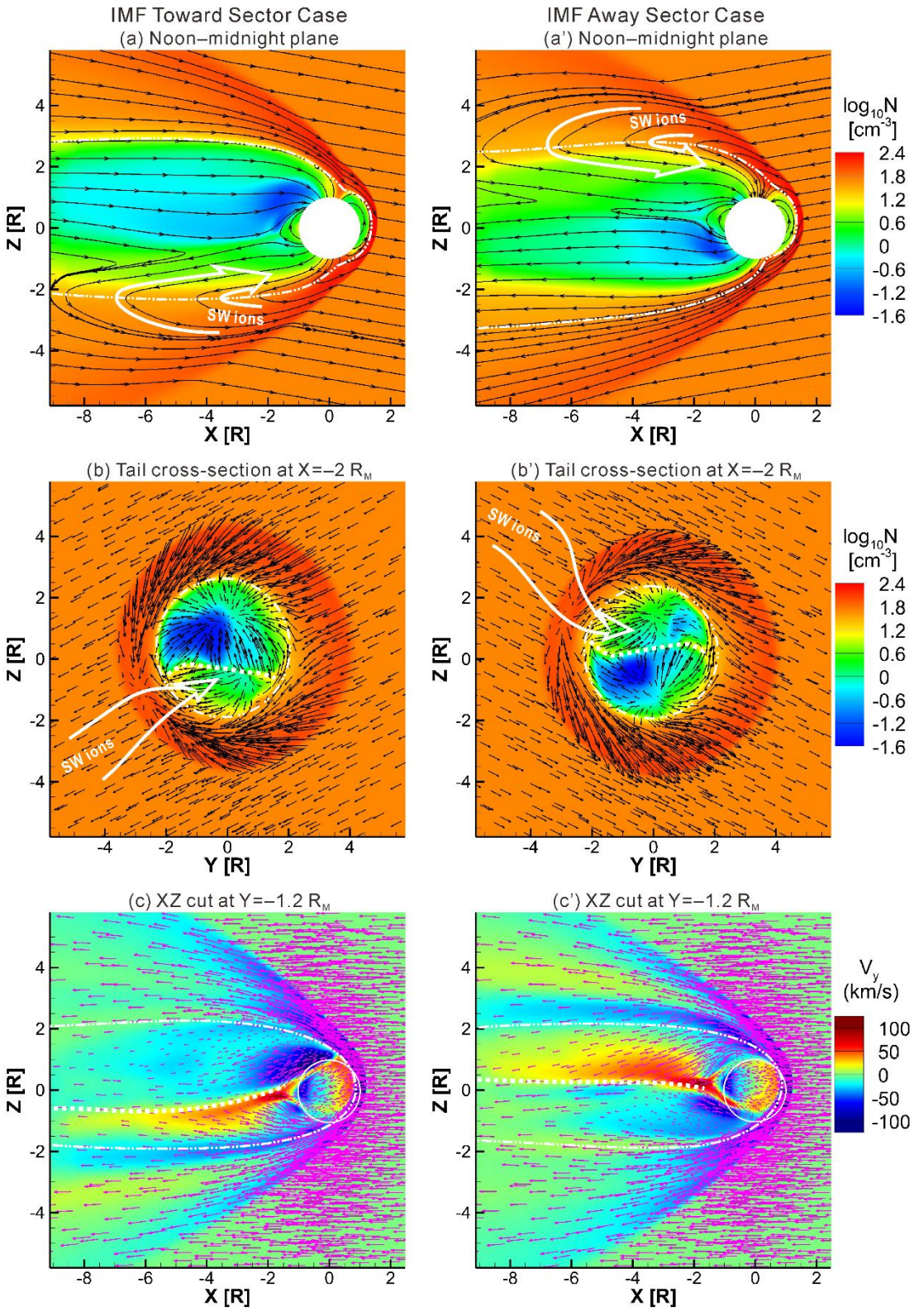



**Figure 4.** Global MHD simulation results for the IMF toward and away sector cases. (a, a') Projected magnetic field lines in the noon-midnight plane. (b, b') Projected magnetic field vectors in YZ cut at X = −2 $R_M$. Color contours: number densities. (c,

This article is protected by copyright. All rights reserved.

Author Manuscript

c') Projected ion flow vectors in XZ cut at Y = −1.2 $R_M$ with dawn-dusk flow in color contours. Thin white dashed lines: magnetopause; Thick white dotted lines: current sheet; Large white arrows: schematic diagram of the entry channel of solar wind ions into the tail along the magnetic field.

From the simulations, it is evident that solar wind can penetrate deep into the near-Mercury tail region under strong IMF conditions. For the IMF toward sector, the southern lobe is interconnected to the upstream solar wind and packed with dense solar wind ions (Figure 4a). This north–south asymmetry is reversed for the IMF away sector (Figure 4a'). The north–south plasma asymmetries observed across the near-tail current sheet are reproduced in the simulation. As shown in the tail cross-section at X = −2 $R_M$, these asymmetries are clearly across the tail current sheet on the dawnside in both cases (Figure 4b and 4b').

The open magnetopause exhibits a clear rotational discontinuity. Across the rotational discontinuity, the component of the ion flow along the magnetic field from the solar wind into the magnetosphere proceeds with the Alfvén velocity (denoted by large white arrow in Figure 4a and 4a') (*Lee and Roederer*, 1982). The simulations reproduced such inward ion flow from solar wind into magnetosphere in the southern tail for the IMF toward sector (Figure 4c) and in the northern tail for the IMF away sector (Figure 4c'). Owing to the Parker spiral configuration, the upstream solar wind enters the magnetosphere from the dawnside in both cases (+$V_Y$, Figure 4c and 4c'). Additionally, for the IMF toward sector, the magnetic field on the dawnside of the southern lobe constitutes a strong dawnward component (−$B_Y$, Figure 4b), whereas the magnetic field has a duskward component (+$B_Y$) in the northern lobe for the IMF away sector (Figure 4b'); these results are consistent with the observations. This is caused by the presence of IMF $B_Y$, which results in magnetic dragging toward dawn in both cases. Both Parker spiral configuration and magnetic dragging result in a dawnside preference of these north–south asymmetry events.

This article is protected by copyright. All rights reserved.

Author Manuscript

## 4 Discussion

Mercury's weak and small magnetosphere, driven by a strong IMF, probably causes solar wind to enter the magnetosphere in a different manner from that of Earth. At Earth, solar wind entering is dominated by IMF $B_Z$. When the IMF is southward, solar wind can enter the tail lobes in the form of plasma mantle, and it is asymmetric between the northern and southern lobes depends on the IMF $B_Y$ direction, i.e., in the northern-dawn and southern-dusk quadrants of the tail lobes when $B_Y > 0$ and in the other two quadrants when $B_Y < 0$ (*Gosling et al.*, 1985; *Wang et al.*, 2022). When the IMF is northward, solar wind plasma can enter the plasma sheet through high-latitude double-cusp reconnections, forming a low-latitude boundary layer (*Le et al.*, 1996) and a relatively thick and dense plasma sheet (*Song and Russell*, 1992). North–south asymmetry of solar wind entry events in the lobes was also observed during quiet times, and it was modulated by the magnetic dipole tilt and Parker spiral of the IMF (*Shi et al.*, 2013; *Gou et al.*, 2016). At Mercury, however, solar wind preferentially enters the near-tail region in one hemisphere under strong IMF conditions. Under such conditions, north–south asymmetry in the two duskside quadrants becomes less apparent or disappears. Due to the close proximity of Mercury's orbit to the Sun, the IMF has a greater intensity and more radial orientation than at Earth's orbit. Our results suggest that the Parker spiral IMF with a dominating radial component creates strong north–south and dawn–dusk asymmetries in the solar wind entering the near-Mercury tail.

Additionally, Mercury's northward offset dipole field may alter the efficiency of solar wind entering the two hemispheres. Both proton-reflection magnetometry (*Winslow et al.*, 2014) and data-based magnetopause model (*Zhong et al.*, 2015) have predicted that solar wind can directly access most of Mercury's southern hemisphere surface. In our simulations, the influence of the offset dipole field on the north–south asymmetry was not obvious in the near magnetotail ($X > -4\ R_M$). However, in the mid- and distant-tail regions beyond $X \sim -4\ R_M$, solar wind ions also filled the

This article is protected by copyright. All rights reserved.

Author Manuscript

southern hemisphere for the IMF away sector. As a result, the north–south plasma asymmetry was not evident, whereas the asymmetry for the IMF toward sector remained. Comparing the northern lobe in the IMF toward sector case (Figure 4a) and southern lobe in the IMF away sector case (Figure 4a'), it appears that the solar wind can enter the southern lobe more easily. This may explain the more solar wind-entering events in the southern lobe.

## 5 Summary

Both observations and simulations suggest that solar wind ions can enter deep into the near-Mercury tail and have direct contact with the tail current sheet in one hemisphere under strong IMF conditions. The IMF sector structures are crucial for the hemispheric asymmetry of the plasma and energy transfer from the solar wind to Mercury's magnetosphere. This asymmetry may be modified by the northward offset dipole field in the mid- or distant-tail regions. One consequence is the involvement of asymmetric reconnection, or the formation of a rotational discontinuity in the near-tail region owing to the significantly different densities on either side of the current sheet. More detailed investigations of magnetotail dynamics and hemispheric asymmetries in magnetosphere–exosphere–surface coupling will be enabled by forthcoming high-resolution observations from the dual spacecraft of the BepiColombo mission (*Milillo et al.*, 2020; *Saito et al.*, 2021).

## Acknowledgments

This work was supported by the B-type Strategic Priority Program of the Chinese Academy of Sciences (grant No. XDB41000000), the National Natural Science Foundation of China (42174217), and the Key Research Program of the Institute of Geology & Geophysics, CAS (Grant No. IGGCAS-201904 and IGGCAS-202102). L. C. Lee was supported by the Ministry of Science and Technology, Taiwan (MOST 110-2111-M-002-017). J. A. Slavin acknowledges support from NASA grants 80NSSC18K1137, 80NSSC21M0364 and 80NSSC21K0052. L. Xie is supported by

This article is protected by copyright. All rights reserved.

Author Manuscript

the Youth Innovation Promotion Association of the Chinese Academy of Sciences. We acknowledge the CSEM team at the University of Michigan for the use of the SWMF tool. Especially, we acknowledge Xianzhe Jia for his pioneer work on the global MHD simulation of Mercury's magnetosphere.

## Open Research

MAG data are publicly available in Raines (2017). FIPS data are publicly available in Korth (2021). The list of 202 Mercury's near-tail current sheet events is available in Zhong (2023).

## References

Anderson, B. J., M. H. Acuña, D. A. Lohr, J. Scheifele, A. Raval, H. Korth, and J. A. Slavin (2007), The Magnetometer instrument on MESSENGER, *Space Sci. Rev.*, *131*(1-4), 417-450, https://doi.org/10.1007/s11214-007-9246-7.

Anderson, B. J., C. L. Johnson, H. Korth, M. E. Purucker, R. M. Winslow, J. A. Slavin, S. C. Solomon, R. L. McNutt, J. M. Raines, and T. H. Zurbuchen (2011), The global magnetic field of Mercury from MESSENGER orbital observations, *Science*, *333*(6051), 1859-1862, https://doi.org/10.1126/science.1211001.

Andrews, G. B., et al. (2007), The Energetic Particle and Plasma Spectrometer instrument on the MESSENGER spacecraft, *Space Sci. Rev.*, *131*(1-4), 523-556, https://doi.org/10.1007/s11214-007-9272-5.

Dewey, R. M., J. M. Raines, W. Sun, J. A. Slavin, and G. Poh (2018), MESSENGER Observations of Fast Plasma Flows in Mercury's Magnetotail, *Geophy. Res. Lett.*, *45*(19), 10,110-110,118, https://doi.org/https://doi.org/10.1029/2018GL079056.

Dewey, R. M., J. A. Slavin, J. M. Raines, A. R. Azari, and W. Sun (2020), MESSENGER Observations of Flow Braking and Flux Pileup of Dipolarizations in Mercury's Magnetotail: Evidence for Current Wedge Formation, *J. Geophys. Res. Space Physics*, *125*(9), e2020JA028112, https://doi.org/10.1029/2020ja028112.

DiBraccio, G. A., J. A. Slavin, S. A. Boardsen, B. J. Anderson, H. Korth, T. H. Zurbuchen, J. M. Raines, D. N. Baker, R. L. McNutt, and S. C. Solomon (2013), MESSENGER observations of magnetopause structure and dynamics at Mercury, *J. Geophys. Res. Space Physics*, *118*, 997-1008, https://doi.org/10.1002/jgra.50123.

DiBraccio, G. A., et al. (2015), First observations of Mercury's plasma mantle by MESSENGER, *Geophy. Res. Lett.*, n/a-n/a, https://doi.org/10.1002/2015GL065805.

Gershman, D. J., J. A. Slavin, J. M. Raines, T. H. Zurbuchen, B. J. Anderson, H.

This article is protected by copyright. All rights reserved.

Author Manuscript

Korth, D. N. Baker, and S. C. Solomon (2013), Magnetic flux pileup and plasma depletion in Mercury's subsolar magnetosheath, *J. Geophys. Res. Space Physics*, *118*(11), 2013JA019244, https://doi.org/10.1002/2013JA019244.

Gosling, J. T., D. N. Baker, S. J. Bame, W. C. Feldman, R. D. Zwickl, and E. J. Smith (1985), North-south and dawn-dusk plasma asymmetries in the distant tail lobes: ISEE 3, *Journal of Geophysical Research: Space Physics*, *90*(A7), 6354-6360, https://doi.org/https://doi.org/10.1029/JA090iA07p06354.

Gou, X. C., et al. (2016), Solar wind plasma entry observed by cluster in the high-latitude magnetospheric lobes, *Journal of Geophysical Research: Space Physics*, *121*(5), 4135-4144, https://doi.org/https://doi.org/10.1002/2015JA021578.

James, M. K., S. M. Imber, E. J. Bunce, T. K. Yeoman, M. Lockwood, M. J. Owens, and J. A. Slavin (2017), Interplanetary magnetic field properties and variability near Mercury's orbit, *J. Geophys. Res. Space Physics*, *122*(8), 7907-7924, https://doi.org/doi:10.1002/2017JA024435.

Jasinski, J. M., J. A. Slavin, J. M. Raines, and G. A. DiBraccio (2017), Mercury's Solar Wind Interaction as Characterized by Magnetospheric Plasma Mantle Observations With MESSENGER, *J. Geophys. Res. Space Physics*, *122*(12), 12,153-112,169, https://doi.org/10.1002/2017ja024594.

Jia, X., J. A. Slavin, T. I. Gombosi, L. K. S. Daldorff, G. Toth, and B. van der Holst (2015), Global MHD simulations of Mercury's magnetosphere with coupled planetary interior: Induction effect of the planetary conducting core on the global interaction, *J. Geophys. Res. Space Physics*, *120*(6), 2015JA021143, https://doi.org/10.1002/2015JA021143.

Korth, H. (2021). MESSENGER MAG Calibrated MSO Coordinates Science Data Collection [Dataset]. NASA Planetary Data System. https://doi.org/10.17189/1522385.

Le, G., C. T. Russell, J. T. Gosling, and M. F. Thomsen (1996), ISEE observations of low-latitude boundary layer for northward interplanetary magnetic field: Implications for cusp reconnection, *Journal of Geophysical Research: Space Physics*, *101*(A12), 27239-27249, https://doi.org/https://doi.org/10.1029/96JA02528.

Lee, L. C., and J. G. Roederer (1982), Solar wind energy transfer through the magnetopause of an open magnetosphere, *Journal of Geophysical Research: Space Physics*, *87*(A3), 1439-1444, https://doi.org/https://doi.org/10.1029/JA087iA03p01439.

Leyser, R. P., S. M. Imber, S. E. Milan, and J. A. Slavin (2017), The Influence of IMF Clock Angle on Dayside Flux Transfer Events at Mercury, *Geophy. Res. Lett.*, *44*(21), 10,829-810,837, https://doi.org/10.1002/2017gl074858.

Milillo, A., et al. (2020), Investigating Mercury's Environment with the Two-Spacecraft BepiColombo Mission, *Space Sci. Rev.*, *216*(5), 93,

This article is protected by copyright. All rights reserved.

Author Manuscript

https://doi.org/10.1007/s11214-020-00712-8.

Poh, G., et al. (2016), MESSENGER observations of cusp plasma filaments at Mercury, *J. Geophys. Res. Space Physics*, *121*(9), 8260-8285, https://doi.org/doi:10.1002/2016JA022552.

Poh, G., J. A. Slavin, X. Jia, J. M. Raines, S. M. Imber, W.-J. Sun, D. J. Gershman, G. A. DiBraccio, K. J. Genestreti, and A. W. Smith (2017), Mercury's cross-tail current sheet: Structure, X-line location and stress balance, *Geophy. Res. Lett.*, *44*(2), 678-686, https://doi.org/10.1002/2016GL071612.

Raines, J. M., et al. (2022), Proton Precipitation in Mercury's Northern Magnetospheric Cusp, *J. Geophys. Res. Space Physics*, *127*(11), e2022JA030397, https://doi.org/https://doi.org/10.1029/2022JA030397.

Raines, J. M., D. J. Gershman, J. A. Slavin, T. H. Zurbuchen, H. Korth, B. J. Anderson, and S. C. Solomon (2014), Structure and dynamics of Mercury's magnetospheric cusp: MESSENGER measurements of protons and planetary ions, *J. Geophys. Res. Space Physics*, *119*, 6587-6602, https://doi.org/10.1002/2014JA020120.

Raines, J. M., J. A. Slavin, T. H. Zurbuchen, G. Gloeckler, B. J. Anderson, D. N. Baker, H. Korth, S. M. Krimigis, and R. L. McNutt Jr (2011), MESSENGER observations of the plasma environment near Mercury, *Planet. Space Sci.*, *59*(15), 2004-2015, https://doi.org/http://dx.doi.org/10.1016/j.pss.2011.02.004.

Raines, J. (2017). MESSENGER EPPS FIPS Derived Data Archive [Dataset]. NASA Planetary Data System. https://doi.org/10.17189/1519743.

Saito, Y., et al. (2021), Pre-flight Calibration and Near-Earth Commissioning Results of the Mercury Plasma Particle Experiment (MPPE) Onboard MMO (Mio), *Space Sci. Rev.*, *217*(5), 70, https://doi.org/10.1007/s11214-021-00839-2.

Shi, Q. Q., et al. (2013), Solar wind entry into the high-latitude terrestrial magnetosphere during geomagnetically quiet times, *Nat Commun*, *4*, 1466, https://doi.org/https://doi.org/10.1038/ncomms2476.

Slavin, J. A., and R. E. Holzer (1979), The effect of erosion on the solar wind stand-off distance at Mercury, *J. Geophys. Res. Space Physics*, *84*(A5), 2076-2082, https://doi.org/10.1029/JA084iA05p02076.

Slavin, J. A., et al. (2012), MESSENGER observations of a flux-transfer-event shower at Mercury, *J. Geophys. Res. Space Physics*, *117*(A12), A00M06, https://doi.org/10.1029/2012ja017926.

Slavin, J. A., S. M. Imber, and J. M. Raines (2021), *A Dungey Cycle in the Life of Mercury's Magnetosphere*, American Geophysical Union, Magnetospheres in the Solar System.

Slavin, J. A., et al. (2010), MESSENGER observations of large flux transfer events at

This article is protected by copyright. All rights reserved.

Author Manuscript

Mercury, *Geophy. Res. Lett.*, *37*(2), L02105, https://doi.org/10.1029/2009GL041485.

Song, P., and C. T. Russell (1992), Model of the formation of the low-latitude boundary layer for strongly northward interplanetary magnetic field, *Journal of Geophysical Research: Space Physics*, *97*(A2), 1411-1420, https://doi.org/https://doi.org/10.1029/91JA02377.

Sun, W. J., et al. (2020), Flux Transfer Event Showers at Mercury: Dependence on Plasma β and Magnetic Shear and Their Contribution to the Dungey Cycle, *Geophy. Res. Lett.*, *47*(21), e2020GL089784, https://doi.org/https://doi.org/10.1029/2020GL089784.

Tóth, G., et al. (2012), Adaptive numerical algorithms in space weather modeling, *Journal of Computational Physics*, *231*(3), 870-903, https://doi.org/https://doi.org/10.1016/j.jcp.2011.02.006.

Wang, C.-P., X. Xing, X. Wang, L. A. Avanov, Y. Lin, R. J. Strangeway, and H. Y. Wei (2022), Effect of IMF By on the Entry of Solar Wind Ions Into the Near-Earth Tail Lobe: Global Hybrid Simulation and MMS Observation, *Journal of Geophysical Research: Space Physics*, *127*(9), e2022JA030800, https://doi.org/https://doi.org/10.1029/2022JA030800.

Winslow, R. M., B. J. Anderson, C. L. Johnson, J. A. Slavin, H. Korth, M. E. Purucker, D. N. Baker, and S. C. Solomon (2013), Mercury's magnetopause and bow shock from MESSENGER Magnetometer observations, *J. Geophys. Res. Space Physics*, *118*, 2213-2227, https://doi.org/10.1002/jgra.50237.

Winslow, R. M., et al. (2014), Mercury's surface magnetic field determined from proton-reflection magnetometry, *Geophy. Res. Lett.*, *41*(13), 4463-4470, https://doi.org/doi:10.1002/2014GL060258.

Zhong, J., L.-C. Lee, J. A. Slavin, H. Zhang, and Y. Wei (2023), MESSENGER Observations of Reconnection in Mercury's Magnetotail Under Strong IMF Forcing, *J. Geophy. Res. Space Physics*, *128*(2), e2022JA031134, https://doi.org/https://doi.org/10.1029/2022JA031134.

Zhong, J., W. X. Wan, J. A. Slavin, Y. Wei, R. L. Lin, L. H. Chai, J. M. Raines, Z. J. Rong, and X. H. Han (2015), Mercury's three-dimensional asymmetric magnetopause, *J. Geophy. Res. Space Physics*, *120*, 7658-7671, https://doi.org/10.1002/2015JA021425.

Zhong, J., Y. Wei, L. C. Lee, J. S. He, J. A. Slavin, Z. Y. Pu, H. Zhang, X. G. Wang, and W. X. Wan (2020), Formation of Macroscale Flux Transfer Events at Mercury, *Astrophys. J. Lett.*, *893*(1), L18, https://doi.org/10.3847/2041-8213/ab8566.

Zhong, J. (2023). A list of Mercury's near-tail current sheet crossings observed by the MESSENGER spacecraft [Dataset]. Zenodo. https://doi.org/10.5281/zenodo.10082316.

This article is protected by copyright. All rights reserved.